Sensors & Actuators: B. Chemical 360 (2022) 131641

Contents lists available at ScienceDirect

Sensors and Actuators: B. Chemical

journal homepage: www.elsevier.com/locate/snb

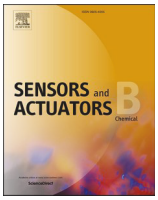

# Analysis of mitochondrial oxygen consumption and hydrogen peroxide release from cardiac mitochondria using electrochemical multi-sensors

Ming-Hao Cheng [a], Adam J. Chicco [b], Daniel Ball [a], Thomas W. Chen [a,c,*]

[a] Department of Electrical and Computer Engineering, Colorado State University, Fort Collins, CO 80523, USA
[b] Department of Biomedical Sciences, Colorado State University, Fort Collins, CO 80523, USA
[c] School of Biomedical Engineering, Colorado State University, Fort Collins, CO 80523, USA

ARTICLE INFO

*Keywords:*
Enzymatic sensor
Hydrogen peroxide sensor
Oxygen sensor
Mitochondria
Biosensors

ABSTRACT

Mitochondria are the primary sites of oxygen ($O_2$) consumption and energy metabolism in most cell types, but also produce reactive oxygen species (ROS) that contribute to a wide array of pathological and physiological processes. Accordingly, simultaneous monitoring of mitochondrial ROS release and oxygen consumption rate (OCR) from cells and mitochondrial preparations is an attractive investigative approach in biological research, particularly when sample quantity is scarce. This paper presents the development of a sensitive multi-sensor device capable of measuring ROS production and OCR from biological samples in a single micro-chamber assay. Sensor sensitivities for $O_2$ and hydrogen peroxide ($H_2O_2$; the major ROS species released by mitochondria and cells) are 4.32 nA/μM and 54.89 nA/μM, respectively, with limits of detection of 2.9 μM and 58.36 nM, respectively. Proof-of-concept studies in isolated mitochondria from rat cardiac tissue (5 μg protein) demonstrate an expected 3 – 4 fold increase in $H_2O_2$ release over the basal rate following addition of respiratory substrates, with a comparatively small change in OCR. The subsequent addition of adenosine diphosphate (ADP) decreased $H_2O_2$ release by 73% ($p < 0.01$) and increased OCR by 168% ($p < 0.01$), consistent with established shifts in mitochondrial membrane potential and electron flow from an ADP-limited (State 4) to ADP-stimulated (State 3) respiratory state. These studies validate the results from the use of a novel multi-sensor device capable of monitoring OCR and $H_2O_2$ simultaneously in scarce biological samples, with potential utility in the non-destructive integrative study of cellular metabolism and mitochondrial function.

## 1. Introduction

Mitochondrial respiration accounts for the majority of oxygen ($O_2$) consumed by living cells, serving as the final electron acceptor to produce water in the oxidative phosphorylation (OXPHOS) of adenosine diphosphate (ADP) to ATP. However, a small proportion of $O_2$ consumed by mitochondria is reduced by single electrons to produce superoxide radicals in the electron transport system [1]. These and other mitochondria-derived reactive oxygen species (ROS) play important roles in physiological cell signaling, but have also been implicated in the development of diabetes [2], cardiovascular disease [3], and neurodegenerative disorders [4]. Most superoxide is rapidly converted to hydrogen peroxide ($H_2O_2$) in the mitochondrial matrix and inner membrane space, where it can readily cross mitochondrial membranes to damage cellular components and trigger cell signaling cascades [5]. The rates of mitochondrial $H_2O_2$ efflux are influenced by a complex interaction of intrinsic and extrinsic factors that vary substantially across cell types, respiratory states, and assay conditions, rather than being a fixed proportion of mitochondrial respiration [6,1,7].

Several methodologies have been developed for monitoring ROS release from various sample types in vitro [8], most commonly utilizing fluorophores such as Amplex® UltraRed to monitor changes in media $H_2O_2$ levels [6,9]. These approaches are typically employed in isolated mitochondria in the absence of ADP (State 4 or "LEAK" respiration), where mitochondria are energized with substrates that maximize mitochondrial ROS production relative to the oxygen consumption rate (OCR) in order to generate the most robust signal [10]. However, the rate of $H_2O_2$ release is much lower during oxidative phosphorylation (State 3 or "OXPHOS-linked" respiration) when OCR is much higher, leading to shifts in the ratio of ROS production and OCR that provide

* Correspondence to: Department of Electrical & Computer Engineering, School of Biomedical Engineering, Colorado State University, Fort Collins, CO 80523, USA.
*E-mail address:* thomas.chen@colostate.edu (T.W. Chen).

https://doi.org/10.1016/j.snb.2022.131641
Received 5 December 2021; Received in revised form 14 February 2022; Accepted 26 February 2022
Available online 28 February 2022

important insight to mitochondrial responses to physiological and pathological stress. Commercial platforms relying on fluorescence intensity measurement, such as Seahorse XF or Synergy HTX, can provide information on mitochondrial oxidative stress via OCR and/or extracellular acidification rate (ECAR) to infer the level of ROS production. However, they do not directly measure ROS production, let alone providing simultaneous measurement of OCR and ROS production to gain better understanding of the relationship between OCR and ROS production under a variety of conditions. Increasing interest in the relationship between cellular ROS production and $O_2$ consumption rates under these dynamic conditions has led to new instrumentation and methodology for simultaneous monitoring of OCR and $H_2O_2$ release from various sample preparations [11,6,12]. However, these new techniques allowing simultaneous monitoring of OCR and $H_2O_2$ production also rely on fluorescence and requires large quantity of biological samples.

The aim of this work was to develop and test a metabolic microsensor technology capable of monitoring OCR and $H_2O_2$ release from small biological samples that could be easily integrated with existing multi-sensor platforms recently described in the literature [13,14]. The sensor device presented in this paper performs simultaneous $O_2$ and $H_2O_2$ measurements electrochemically to allow miniaturization and monitoring results in real-time. We present the design and fabrication of the first metabolic multi-sensor that combines electrochemical and potentiometric sensors capable of monitoring OCR, $H_2O_2$, and pH in the same sample micro-chamber. Given descriptions of the pH sensor in previous publications [14], we have focused our proof-of-concept studies on demonstrating the performance and integration of the $O_2$ and $H_2O_2$ sensors utilizing isolated mitochondria at quantities $< 10\%$ of those routinely used in existing commercial platforms [6,12]. The technical advances presented in this paper have the potential to improve our understanding of cellular ROS production in health and disease, particularly if they can be integrated with other metabolic analyses from the same biological sample.

## 2. Materials and methods

### 2.1. Sensor electrode design, fabrication, and surface modification

A multi-sensor chip was designed with a total of six sensors, five of which are electrochemical type sensors and the sixth sensor is a potentiometric type sensor for pH measurement. One electrochemical sensor was designated for $O_2$ measurement and the other four were designated for $H_2O_2$ measurement. Each electrochemical sensor was designed in a three-electrode electrochemical cell configuration with a working electrode (WE), a reference electrode (RE), and a counter electrode (CE). The RE and CE are shared between $O_2$ and $H_2O_2$ sensors. Both the WEs and CEs are gold electrodes, and the REs are Ag/AgCl electrode.

The multi-sensor chip was fabricated on a 25 mm × 25 mm glass substrate through standard photolithography using S1813 positive photoresist (Megaposit, Dow, USA), the developer of S1813 (Megaposit MF-26A, Dow, USA), and thermal evaporation. Details of photolithography and thermal evaporation can be found in the previous project [13]. Fig. 1A shows a finished multi-sensor chip with each electrode labeled.

The $O_2$ sensor has a 1 mm diameter WE while the $H_2O_2$ sensor has four 1 mm diameter WE's in the four corners of the well electrically shorted to have a larger WE area. After rinsing the sensor surface with methanol and deionized (DI) water followed by 1% Triton X-100 (Sigma-Aldrich, USA) for 20 min, a solid electrolyte layer was formed on the WE surface of the $O_2$ sensor by drop coating 0.1 μl Nafion solution (5% w/w, Sigma-Aldrich, USA) as previously described [15]. The preparation of the WE of the $H_2O_2$ sensor was adapted from [16]. An electropolymerization charge of 35 mC $cm^{-2}$ was applied when polymerizing the electrode with a mixture of horseradish peroxide (Sigma-Aldrich, USA) and pyrrole (Sigma-Aldrich, USA) as conducting polymers. The silver/silver chloride (Ag/AgCl) pseudo-RE was prepared by oxidizing the silver electrodes with 50 mM ferric chloride for 20 min at room temperature. Finally, the sensor was rinsed with deionized water.

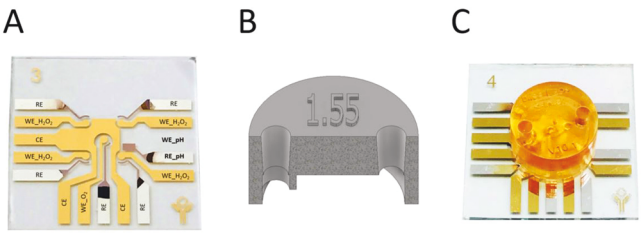


**Fig. 1.** (A) Multi-sensor chip. CE is shared between the $O_2$ sensor and the $H_2O_2$ sensor. WE of the $O_2$ sensor and WE of the $H_2O_2$ sensor are labeled as WE_$O_2$ and WE_$H_2O_2$, respectively, and all WE_ $H_2O_2$'s are shorted externally in order to have a larger WE area. All REs are also shorted externally except for RE_pH which was not used in experiments described in this paper. An ITO-based WE of the pH sensor is labeled as WE_pH, which was not used in the experiments described in this paper either. (B) Microchamber design with an inlet (left) and an outlet (right) on the top. (C) Photo of an actual sensor chip with the microchamber mounted on it.

### 2.2. Microchamber design and fabrication

A microchamber well sits on the multi-sensor glass chip to house cells inside the microchamber during measurement. The microchamber well has an internal volume of 180 μl. Fig. 1B shows the cross-section of the microchamber well design. There is an inlet to the left and an outlet to the right of the well. The inlet has a slightly lower entry point inside the microchamber well to allow media or other therapeutics to reach the cells inside the well better. The tubing from the inlet was attached to a three-way splitter (not shown in Fig. 1) to allow two different therapeutics (i.e. respiration substrate and ADP) to be injected into the microchamber using two syringes. The microchamber well was printed using a stereolithography (SLA) 3D printer with a biocompatible resin (SG, NextDent, Netherlands). The well was then bound to the glass chip with double-sided tape (468MP, 3 M, USA) patterned by a laser cutter (LS1416, Boss Laser, USA). Fig. 1 C shows the microchamber attached to the sensor chip glass substrate.

### 2.3. Printed circuit board and chip holder

The printed circuit board (PCB) was designed and manufactured to provide connections between the electrodes on the multi-sensor glass chip and the external potentiostat. As shown in Fig. 2A, the PCB has a rectangular opening in the middle to accommodate the microchamber well on the multi-sensor glass chip. A set of spring-pin connectors whose pin pitch matches the pitch of the electrode pads at the edge of the multi-sensor glass chip are mounted at the edges of the rectangular opening of the PCB. After mounting the microchamber well on to the glass multi-sensor chip, the glass multi-sensor chip is slid into the PCB to allow the electrodes on the glass chip to make contacts to the PCB via the spring-pin connectors (see Fig. 2B). The connections were further secured by the use of two aluminum chip holder sandwiching the PCB and the multi-sensor glass chip in the middle with four screws to complete the final assembly. The pins of the spring-pin connectors on top of the board (shown in Fig. 2A) were then used for making connections to the external potentiostat (Quadstat EA164H, eDAQ, USA). Fig. 2C shows the final assembly of the multi-sensor chip module ready for measurement.

### 2.4. Mitochondrial isolation

Cardiac mitochondria used in our studies were isolated from adult

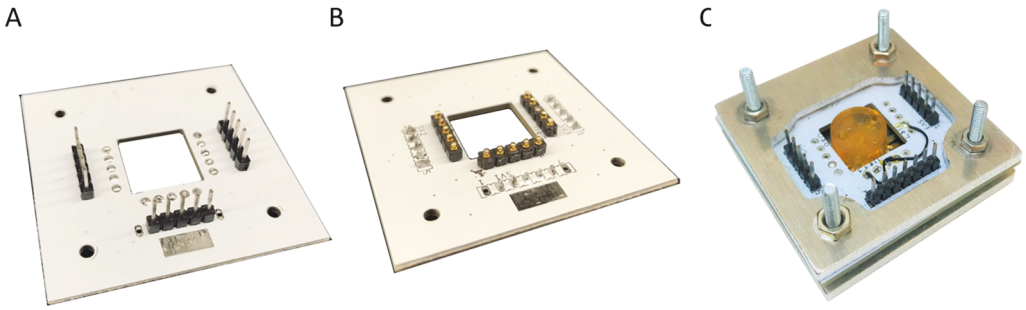


**Fig. 2.** (A) and (B) are the top and bottom side of the PCB, respectively, used for making connections between the glass sensor chip and the external potentiostat. (C) Final assembly of the multi-sensor chip module.

(4–5 month old) male Fischer 344 (CDF) rats obtained from Charles River (Wilmington, MA) housed in a temperature and humidity controlled facility on a 12:12 h light:dark cycle and provided water and chow (Purina 2918) ad libitum. Animals were sacrificed for tissue collection by midline thoracotomy and removal of the heart following confirmation of deep anesthesia by sodium pentobarbital injection (100 mg/kg i.p.) using procedures approved by the Colorado State University Care and Use Committee and conform to the Guide for the Care and Use of Laboratory Animals published by the U.S. National Institutes of Health (NIH Publication No. 85–23, revised 1996).

Mitochondria were isolated from left ventricular cardiac tissues using standard differential centrifugation methods essentially as previously described [17]. All procedures were performed on ice or controlled at 4 °C immediately upon harvesting fresh tissue. Hearts were excised and trimmed free of connective tissue, atria, and valves to provide myocardial tissue, then rinsed and minced in ice-cold Chappell--Perry (CP1) buffer consisting of (in mM) 100 KCl, 50 MOPS, 1 EDTA, 5 EGTA, 5 $MgSO_4{\cdot}7H_2O$, and 1 ATP, pH 7.4 with KOH. Minced tissue was then homogenized for 10 s at medium speed using a polytron, and incubated in CP1 containing trypsin (~5 mg/g tissue) for 7 min to disrupt myofibrils in order to extract both interfibrillar and subsarcolemmal mitochondria. Trypsinized homogenates were then subjected to 6 passes with glass-Teflon Potter-Elvehjem homogenizer prior to centrifugation at 600 x g. The supernatant (containing mitochondria) was collected and centrifuged at 7000 x g to pellet mitochondria, followed by three 7000 x g clarifying spins in CP1 + 2 mg/ml albumin, then once in stabilization buffer containing 100 mM KCl, 50 mM MOPS, 0.5 mM EGTA. Final mitochondrial pellets were resuspended in KME at a final protein concentration of ~5 μg/μl determined by the bicinchoninic acid (BCA) assay (ThermoScientific).

### 2.5. Respiration buffers and stimuli for isolated mitochondria

Mitochondrial suspensions (5 μg protein) were added to the sensor microchamber containing 180 μl of mitochondrial respiration medium (MiR05) containing (in mM) 0.5 EGTA, 3 $MgCl_2$ hexahydrate, 60 lactobionic acid, 20 taurine, 10 $KH_2PO_4$, 20 HEPES, 110 sucrose, and 0.1% BSA, pH 7.1 with KOH, which was selected based on rigorous testing that determined this formulation to have the highest stability and sensitivity for simultaneous OCR and $H_2O_2$ measurements [18], and prior use in other metabolic multi-sensor platforms [13,14]. For our proof-of-concept studies, we selected an experimental protocol used to evaluate the relationship between OCR and hydrogen peroxide production rate (HPR) by energized mitochondria during the metabolic shift from a high-membrane potential/low ATP demand (LEAK) state to a lower-membrane potential/high ATP demand (OXPHOS) state [6].

To account for potential interactions between the sensor and the mitochondrial respiration medium, baseline measurements were performed before each measurement without any mitochondria present at the sensor site and were subtracted from the $O_2$ and $H_2O_2$ measurements obtained with mitochondria present. Following a baseline stabilization period, mitochondria were energized with saturating concentrations of substrates that fully reconstitute forward flux of the citric acid cycle, supplying electrons to the mitochondrial respiratory chain through Complexes I and II (in mM): 1 malate, 5 pyruvate, 10 glutamate, and 20 succinate. Flux was then recorded until it stabilized to establish OCR and HPR under LEAK state conditions, after which time ADP (2.5 mM) was added to establish OCR and HPR in the OXPHOS state. With the in-situ baseline calibration method, the data presented were based on the net increase from $H_2O_2$ release from superoxide production inside mitochondria. Previous studies have described these potential interactions in other $H_2O_2$ assay platforms, correcting for them by similar calibration experiments [6].

### 2.6. Sensor activation voltages

Activation voltages used in amperometry for both $O_2$ and $H_2O_2$ measurement were obtained from cyclic voltammetry (CV) data with a scan rate of 100 mV/s. Four $O_2$ concentrations (100%, 70%, 35%, and 0%) were used with each concentration having 5 repeats. Samples were prepared by bubbling nitrogen gas to deionized water and the resulting $O_2$ concentration was confirmed by using a commercial oxygen meter (DO6 +, Oakton, USA). The CV curves for $H_2O_2$ sensor were obtained using solutions made with phosphate-buffered saline and $H_2O_2$ solution (Sigma-Aldrich, USA). The solutions were prepared by diluting a known $H_2O_2$ concentration solution to the concentrations needed for performing CV. A total of 5 concentrations (11 μM, 2.76 μM, 690 nM, 172.5 nM, and 0 nM) were used for obtaining the activation voltage.

### 2.7. Sensors calibration

#### 2.7.1. Oxygen sensor calibration

Using the activation voltage for $O_2$, the calibration curve for $O_2$ were obtained using amperometry with 6 different concentrations. Similar to performing CV, different concentrations of dissolved oxygen (DO) were prepared by bubbling nitrogen gas into the deionized water to adjust the DO level in the solution and the resulting $O_2$ concentrations were confirmed by using a commercial oxygen meter (DO6 +, Oakton, USA). The reduction current for $O_2$ was measured with five sample points ($n = 5$) per concentration at the activation voltage vs. Ag/AgCl with a drift less than 5% over 3 min. Due to the average barometric pressure of the experiment location (Fort Collins, Colorado (84.8 kPa)) at 38.5 °C, the calibration curve was calculated at 158 μM for 21% dissolved oxygen concentration.

#### 2.7.2. Hydrogen peroxide sensor calibration

Similar to performing CV for $H_2O_2$, the $H_2O_2$ sensor was calibrated with solutions made with phosphate-buffered saline and $H_2O_2$ solution (Sigma-Aldrich, USA). The calibration solutions were prepared by diluting a known $H_2O_2$ concentration solution to the concentrations needed in the calibration. Electrochemical amperometry was used to continuously detect change of analyte concentration. There were a total

of 11 concentrations (3.3 μM, 2.2 μM, 1.5 μM, 970 nM, 645 nM, 400 nM, 267 nM, 178 nM, 119 nM, 79 nM, and 0 nM) used for $H_2O_2$ calibration. The oxidative current was measured with five sample points (n = 5) per concentration at the activation voltage vs. Ag/AgCl at 38.5 °C. Each measurement was taken when the measured current had a drift less than 5% over 3 min.

### 2.8. Experimental protocols

The multi-sensor glass chip and its assembly were placed in an incubator with the temperature set at 38.5 °C. A breakout board with relays was used for electrically isolating the WE in use from the other idling WE. The experiments were carried out initially in the oxygen-saturated Mir05 buffer with 1 μl of isolated mitochondria. A decreasing DO concentration was observed due to the $O_2$ consumption of the mitochondria at their basal state. In order to limit the impact of changes in DO concentration on ROS production, the measurement time for $O_2$ was limited to 5 min. A three-way splitter was used to provide injections of substrates and ADP from two different syringes. To minimize the interference from the diffusion of the ambient oxygen, the outlet was normally closed except for during the injection of substrates or ADP. Fig. 3 shows the experiment setup with different components labeled.

After the sensors reached its steady basal state with a known amount of mitochondria in the microchamber, the mitochondria were first energized with 1 μl of substrates from the syringe through the inlet to boost the $H_2O_2$ production rate. Once a stable oxidation current was observed, the measurement of the sensor device was switched to the $O_2$ channel to measure the corresponding DO level. The mitochondria were, then, energized with 1 μl of ADP from the other syringe through the inlet to establish stable OXPHOS-linked OCR and ROS production. Finally, the measurement was switched back to the $H_2O_2$ channel after measuring DO level for five minutes.

The conversion from the measured current to HPR and OCR was performed based on the method adapted from our previous paper [19]:

$$\text{Rate}\left(\text{pmol}\bullet\text{s}^{-1}\bullet\text{mg}^{-1}\right) = \frac{\Delta I/\Delta t}{\Delta I/\Delta C} \times V \times N \div w$$

where N is the quantity of the mitochondria and w is the weight of the mitochondria added into the chamber. The quantity of the mitochondria is 120,000, and the weight of the mitochondria is 5 μg.

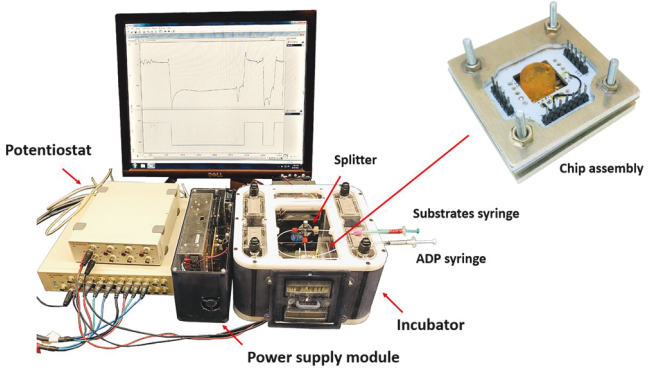


**Fig. 3.** The setup of the measurement system consisting of a customized incubator, syringes for injecting therapeutics, a three-way splitter, the sensor chip assembly, and a potentiostat.

## 3. Results and discussion

### 3.1. Sensors calibration

#### 3.1.1. Hydrogen peroxide sensor calibration

Cyclic voltammetry (CV) was performed in the presence of 11 μM, 2.76 μM, 690 nM, 172.5 nM, and 0 nM of hydrogen peroxide from 0.55 V to 1.05 V with a scan rate of 100 $mV\bullet s^{-1}$ to find the activation voltage of the $H_2O_2$ sensor, and the results are shown in Fig. 4(A). An oxidation peak was observed at 0.4 V for the solutions containing $H_2O_2$, and CV did not present any peak when no $H_2O_2$ was present in the solution. Since the $H_2O_2$ concentration produced by mitochondria was expected to be below 3 μM, an activation voltage of 0.4 V vs. Ag/AgCl was chosen as the activation voltage for calibration and was used for measurement. Fig. 4(B) depicts the amperometric measurement results with eleven different concentrations (0 nM, 3.3 μM, 2.2 μM, 1.5 μM, 970 nM, 645 nM, 400 nM, 267 nM, 178 nM, 119 nM, and 79 nM). All CV's and calibrations of the $H_2O_2$ sensor were carried out at 38.5 °C, which is the same temperature used in the mitochondria measurement described in this article.

A linear calibration curve for the $H_2O_2$ sensor is shown in Fig. 4(B) using the activation voltage of 0.4 V vs. Ag/AgCl. The amperometric current increases linearly with the increase in $H_2O_2$ concentration, and the sensor sensitivity is 54.889 nA/μM with an $R^2$ value of 92.96%. The calibration data (mean ± standard deviation, n = 5) are presented as measured current with respect to $H_2O_2$ concentration in μM. The calculated limit of detection (LoD) of the $H_2O_2$ sensor is 58.36 nM [20].

#### 3.1.2. Oxygen sensor calibration

CV experiments with various oxygen concentrations (100%, 70%, 35%, and 0%) were performed with a scan rate of 100 $mV\bullet s^{-1}$. Based on the CV data shown in Fig. 5(A), the activation voltage for $O_2$ amperometry was found to be − 0.65 V vs. Ag/AgCl. The results of $O_2$ amperometry under six different DO concentrations (100%, 80%, 60% 40%, 20%, and 0%) were shown in Fig. 5(B) and presented as mean ± standard deviation (n = 5). The magnitude of sensor output current increases linearly with the increase of DO concentration. Fig. 5(B) shows the calibration curve of the $O_2$ sensor after converting DO concentration in the chamber from percentage to molarity, where 100% dissolved oxygen concentration represents 158 μM based on the altitude where the experiments were performed. Sensitivity of the $O_2$ sensor when an activation voltage of − 0.65 V vs. Ag/AgCl was applied is − 4.32 nA/μM with an $R^2$ value of 96%, and its calculated LoD is − 143 nA, which is equivalent to 2.9 μM. All CV's and calibrations of the $O_2$ sensor were carried out at 38.5 °C, which is the same temperature used in all mitochondria measurements.

### 3.2. Isolated mitochondria HPR and OCR in LEAK and OXPHOS-linked states

After reaching a stable basal state, the mitochondria were provided substrates to induce maximal non-phosphorylating respiration, commonly referred to as State 4 or LEAK respiration. This was followed by the addition of ADP to maximally fuel the ATP synthase, thus enabling the maximal OXPHOS-linked (or State 3) respiration rate. Fig. 6 shows the changes of HPR and OCR of mitochondria during the transitions from the basal state to the LEAK state, and to the OXPHOS-linked state. OCR did not change significantly from basal to LEAK state (53%). However, it increased 167.94% from 2944.96 $pmol\bullet s^{-1}\bullet mg^{-1}$ to 7890.51 $pmol\bullet s^{-1}\bullet mg^{-1}$ from the LEAK state to the OXPHOS state (Fig. 6A and C), consistent with high respiratory control of cardiac mitochondria by ADP [6]. In contrast, the HPR increased over 350% from the basal state to the LEAK state when mitochondria were energized by substrates (LEAK), then decreased 73.29% from 257.9 $pmol\bullet s^{-1}\bullet mg^{-1}$ to 68.89 $pmol\bullet s^{-1}\bullet mg^{-1}$ ($P < 0.01$) following the transition to the OXPHOS state (Fig. 6 A and

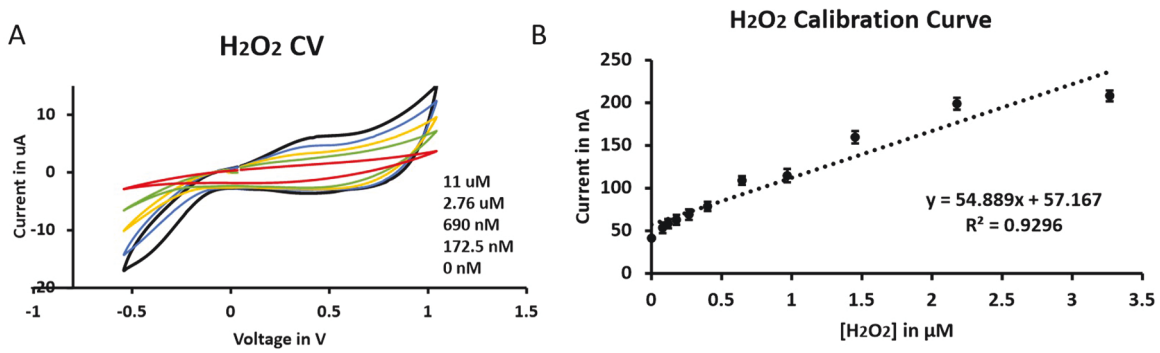


**Fig. 4.** (A) CV results with various [$H_2O_2$]: 11 μM, 2.76 μM, 690 nM, 172.5 nM, and 0 nM. The oxidative peaks are found at 0.4 V. (B) Hydrogen peroxide sensor calibration curve: $H_2O_2$ sensor was calibrated from 0 nM to 3.3 μM. The error bars represent standard deviations (n = 5) measured at 38.5 °C.

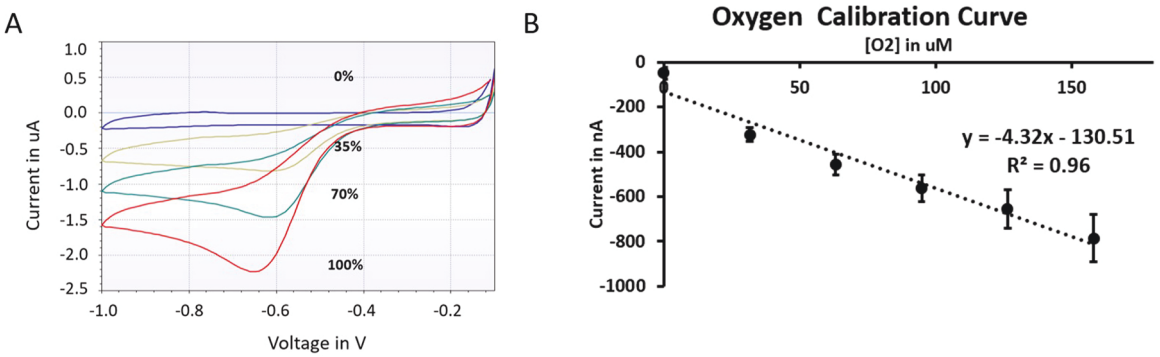


**Fig. 5.** (A) CV results for $O_2$. The reductive peaks of dissolved oxygen can be found around − 0.65 V vs. Ag/AgCl for $O_2$. (B) Oxygen sensor calibration curve: The error bars represent standard deviations (n = 5) measured at 38.5 °C.

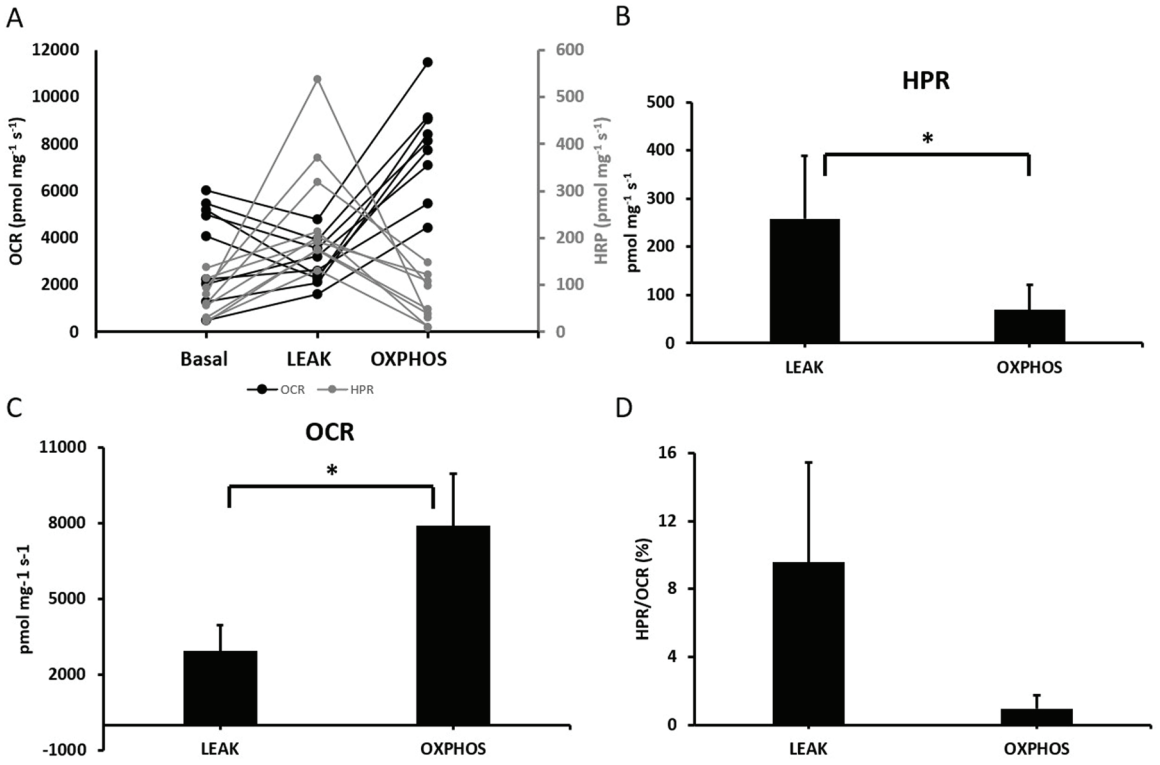


**Fig. 6.** (A) Values of oxygen consumption rate (OCR, black) and hydrogen production rate (HPR, grey) from rat cardiac preparations during basal, LEAK, and OXPHOS-linked respiration. Rates of (B) hydrogen production, (C) oxygen consumption from isolated mitochondria, and (D) ratios of HPR over OCR during LEAK and OXPHOS-linked respiration. Data are presented as mean ± SD (n = 9 for both OCR and HPR and * $p < 0.01$).

6B). This trend is consistent with the strong influence of mitochondrial membrane potential on ROS production by the respiratory chain, which is highest during the LEAK state and dissipated by the activity of ATP synthase in the OXPHOS state [1,6]. The HPR of the mitochondria were about 9.57% of OCR during LEAK, and decreased to 0.95% of OCR during OXPHOS-linked respiration (Fig. 6D), which is similar to the 10-fold decrease in HPR/OCR recently reported from murine cardiac mitochondria using the same protocol using high-resolution fluo-respirometry [6]. Taken together, these results demonstrate the expected responses of intact mitochondrial OCR and HPR to respiratory substrates in the presence and absence of ADP, thereby establishing the utility of this novel multi-sensor device for evaluating mitochondrial bioenergetics in very small biological samples.

Importantly, we would like to note that the HPR has a strong relationship with the $O_2$ concentration in the environment [6]. Mitochondria produce more ROS when $O_2$ concentration is high, and vice versa. This can lead to wide variations in HPR measurements as chamber oxygen declines. We observed that the OCR measurement occasionally could not provide a stable reading within five minutes and the measurement for $O_2$ had to be extended for a maximum of 2 more minutes to allow the readings to stabilize. The longer the $O_2$ measurement time was extended, the less $O_2$ was in the environment due to the $O_2$ consumption by the mitochondria. This could partially explain some of the measurement variations shown in Fig. 6.

### 3.3. Applications for simultaneous monitoring of mitochondria HPR and OCR

ROS are inevitable by-products of mitochondrial respiration, which leave mitochondria and intact cells primarily in the form of $H_2O_2$. Excessive ROS production can be damaging to cells and their tissue environment, contributing to the development and progression of major diseases including cancer and cardiovascular disease. Given their strong interdependence, simultaneous measurement of mitochondrial both OCR and HPR provides more complete information about cell physiology and pathophysiology. The sensor device in this paper demonstrated its ability to simultaneously monitor changes in $H_2O_2$ and $O_2$ concentrations in a small quantity of isolated cardiac mitochondria during the LEAK and OXPHOS-linked respiration. Results illustrate that the multi-sensor platform has the sufficient sensitivities and linearities necessary for both $H_2O_2$ and $O_2$ to enable advances in instrumentation technology that can improve our understanding of cellular bioenergetics in health and disease.

Integration of $O_2$ and $H_2O_2$ sensors in the current device with other metabolic sensors in the same platform [13,14] can provide even more complete information about cellular activity and metabolism. For example, although not used in the present study, a pH sensor can be added to provide simultaneous measurement of extracellular acidification rate (ECAR; a surrogate measure of glycolysis) along with OCR and ROS production from the same biological sample. This approach would be particularly useful for investigating metabolic transitions that occur in several cell types in response to stress, such as immune cells that shift from OXPHOS to glycolytic metabolism when activated by antigen or pathogen [21] or in cancer [22]. These transitions are frequently associated with robust changes in cellular ROS production and release [23], but the precise links between these processes are not well understood. In these contexts, simultaneous measurement of OCR and HPR provides an internally-controlled index of ROS release (HPR/OCR) that is particularly useful for studying samples with inherent or unknown variability in mitochondrial content or metabolic activity, such as primary circulating immune cell samples [24] and heterogeneous tumor micro-biospies [25].

## 4. Conclusions and future work

Metabolic multi-sensors enable an integration of bioenergetic assessments from a single sample, which has the potential to advance clinical and scientific research into immunologic and infectious diseases, cancer, and cardiometabolic disorders. The device presented herein faciliates simultaneous measurement of OCR and HPR, thus providing an opportunity to monitor relative shifts in metabolic flux and ROS production from very small biological samples. This technology is compatible with existing micro-metabolic multi-sensor platforms. However, the close proximity of sensors is prone to sensor-sensor interference, especially when sensors using similar enzymatic mechanisms, such as using glocose oxidase for glocose sensor and lactate oxidase for lactate sensor, respectively. The method presented in this paper by subtracting the baseline amperometric current from current measurements when mitochondria were present may be sufficient for $O_2$ and $H_2O_2$ measurements, fully integrating the present device with those having other sensor types, such as glucose and lactate sensors, will require additional design considerations to minimize the impact of sensor-sensor interferences. A new device design incorporating changes to minimize sensor-sensor interferences to allow simultaneous measurements of more metabolites should lead to new biological insights in the study of cellular metabolism and mitochondrial function in health and disease.

## CRediT authorship contribution statement

**Ming-Hao Cheng:** Methodology, Investigation, Writing – review & editing. **Adam J. Chicco:** Methodology, Conceptualization, Investigation, Writing – review & editing. **Daniel Ball:** Investigation. **Thomas W. Chen:** Supervision, Conceptualization, Methodology, Writing – review & editing.

## Declaration of Competing Interest

The authors declare that they have no known competing financial interests or personal relationships that could have appeared to influence the work reported in this paper.

## Acknowledgements

Results presented in this paper are based upon collaborative work partially supported by National Science Foundation (USA) Grants no. 0841259 and 1450032. Any opinions, findings, conclusions or recommendations expressed in this paper are those of the author(s) and do not necessarily reflect the views of the National Science Foundation (USA).

## References

[1] M.P. Murphy, How mitochondria produce reactive oxygen species, Biochem. J. 417 (2009) 1–13, https://doi.org/10.1042/BJ20081386.
[2] T. Nishikawa, E. Araki, Impact of mitochondrial ROS production in the pathogenesis of diabetes Mellitus and its complications, Antioxid. Redox Signal. 9 (2007) 343–353, https://doi.org/10.1089/ars.2006.1458.
[3] O.S. Kornfeld, S. Hwang, M.-H. Disatnik, C.-H. Chen, N. Qvit, D. Mochly-Rosen, Mitochondrial reactive oxygen species at the heart of the matter, Circ. Res. 116 (2015) 1783–1799, https://doi.org/10.1161/CIRCRESAHA.116.305432.
[4] X. Wang, W. Wang, L. Li, G. Perry, H. Lee, X. Zhu, Oxidative stress and mitochondrial dysfunction in Alzheimer's disease, Biochim. Biophys. Acta 1842 (2014) 1240–1247, https://doi.org/10.1016/j.bbadis.2013.10.015.
[5] G.P. Bienert, J.K. Schjoerring, T.P. Jahn, Membrane transport of hydrogen peroxide, Biochim. Biophys. Acta 1758 (2006) 994–1003, https://doi.org/10.1016/j.bbamem.2006.02.015.
[6] L.C. Li Puma, M. Hedges, J.M. Heckman, A.B. Mathias, M.R. Engstrom, A.B. Brown, A.J. Chicco, Experimental oxygen concentration influences rates of mitochondrial hydrogen peroxide release from cardiac and skeletal muscle preparations, Am. J. Physio. Regul. Integr. Comp. Physio. 318 (2020) R972–R980, https://doi.org/10.1152/ajpregu.00227.2019.
[7] H.-S. Wong, P.A. Dighe, V. Mezera, P.-A. Monternier, M.D. Brand, Production of superoxide and hydrogen peroxide from specific mitochondrial sites under different bioenergetic conditions, J. Biol. Chem. 292 (2017) 16804–16809, https://doi.org/10.1074/jbc.R117.789271.
[8] S.I. Dikalov, D.G. Harrison, Methods for detection of mitochondrial and cellular reactive oxygen species, Antioxid. Redox Signal. 20 (2014) 372–382, https://doi.org/10.1089/ars.2012.4886.

[9] A.A. Starkov, Measurement of mitochondrial ROS production, in: P. Bross, N. Gregersen (Eds.), Protein Misfolding and Cellular Stress in Disease and Aging, Humana Press, Totowa, NJ, 2010, pp. 245–255.
[10] A. Boveris, B. Chance, The mitochondrial generation of hydrogen peroxide. General properties and effect of hyperbaric oxygen, Biochem. J. 134 (1973) 707–716, https://doi.org/10.1042/bj1340707.
[11] G. Krumschnabel, M. Fontana-Ayoub, Z. Sumbalova, J. Heidler, K. Gauper, M. Fasching, E. Gnaiger, Simultaneous High-Resolution Measurement of Mitochondrial Respiration and Hydrogen Peroxide Production, in: V. Weissig, M. Edeas, (Eds.), Mitochondrial Medicine. Methods in Molecular Biology, Humana Press, New York, NY, 2015, pp. 245–261.
[12] M. Makrecka-Kuka, G. Krumschnabel, E. Gnaiger, High-resolution respirometry for simultaneous measurement of oxygen and hydrogen peroxide fluxes in permeabilized cells, tissue homogenate and isolated mitochondria, Biomolecules 5 (2015) 1319–1338, https://doi.org/10.3390/biom5031319.
[13] Y. Obeidat, G. Catandi, E. Carnevale, A.J. Chicco, A. DeMann, S. Field, T. Chen, A multi-sensor system for measuring bovine embryo metabolism, Biosens. Bioelectron. 126 (2019) 615–623, https://doi.org/10.1016/j.bios.2018.09.071.
[14] Y.M. Obeidat, M.-H. Cheng, G. Catandi, E. Carnevale, A.J. Chicco, T.W. Chen, Design of a multi-sensor platform for integrating extracellular acidification rate with multi-metabolite flux measurement for small biological samples, Biosens. Bioelectron. 133 (2019) 39–47, https://doi.org/10.1016/j.bios.2019.02.069.
[15] Y. Obeidat, T. Chen. Characterization of an $O_2$ sensor using microelectrodes, IEEE, 2016, pp. 1–3. https://doi.org/10.1109/ICSENS.2016.7808460.
[16] T. Tatsuma, M. Gondaira, T. Watanabe, Peroxidase-incorporated polypyrrole membrane electrodes, Anal. Chem. 64 (1992) 1183–1187, https://doi.org/10.1021/ac00034a019.
[17] A.B. Heim, D. Chung, G.L. Florant, A.J. Chicco, Tissue-specific seasonal changes in mitochondrial function of a mammalian hibernator, Am. J. Physio. Regul. Integr. Comp. Physio. 313 (2017) R180–R190, https://doi.org/10.1152/ajpregu.00427.2016.
[18] T. Komlódi, O. Sobotka, G. Krumschnabel, N. Bezuidenhout, E. Hiller, C. Doerrier, E. Gnaiger, Comparison of mitochondrial incubation media for measurement of respiration and hydrogen peroxide production, in: C. Palmeira, A. Moreno (Eds.), Mitochondrial Bioenergetics. Methods in Molecular Biology, Human Press, New York, NY, 2018, pp. 137–155.
[19] Y.M. Obeidat, A.J. Evans, W. Tedjo, A.J. Chicco, E. Carnevale, T.W. Chen, Monitoring oocyte/embryo respiration using electrochemical-based oxygen sensors, Sens. Actuators B: Chem. 276 (2018) 72–81, https://doi.org/10.1016/j.snb.2018.07.157.
[20] D.A. Armbruster, T. Pry, Limit of blank, limit of detection and limit of quantitation, Clin. Biochem. Rev. 29 (Suppl 1) (2008) S49–S52.
[21] Y. Li, A. Jia, Y. Wang, L. Dong, Y. Wang, Y. He, S. Wang, Y. Cao, H. Yang, Y. Bi, G. Liu, Immune effects of glycolysis or oxidative phosphorylation metabolic pathway in protecting against bacterial infection, J. Cell. Physiol. 234 (11) (2019) 20298–20309, https://doi.org/10.1002/jcp.28630.
[22] J. Zheng, Energy metabolism of cancer: Glycolysis versus oxidative phosphorylation, Oncol. Lett. 4 (6) (2012) 1151–1157, https://doi.org/10.3892/ol.2012.928.
[23] H.-Y. Peng, J. Lucavs, D. Ballard, J.K. Das, A. Kumar, L. Wang, Y. Ren, X. Xiong, J. Song, Metabolic reprogramming and reactive oxygen species in T cell immunity, Front. Immunol. 12 (2021), 652687, https://doi.org/10.3389/fimmu.2021.652687.
[24] X. Zhang, A. Mardinoglu, L.A.B. Joosten, J.A. Kuivenhoven, Y. Li, M.G. Netea, A. K. Groen, Identification of discriminating metabolic pathways and metabolites in human PBMCs stimulated by various pathogenic agents, Front. Physiol. 9 (2018), 139, https://doi.org/10.3389/fphys.2018.00139.
[25] S. Loponte, S. Lovisa, A.K. Deem, A. Carugo, A. Viale, The many facets of tumor heterogeneity: is metabolism lagging behind? Cancers 11 (10) (2019) 1574, https://doi.org/10.3390/cancers11101574.

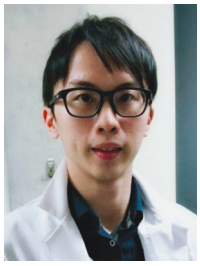

**Ming-Hao Cheng** received the B.S. and M.S. in Electrical Engineering from Chang Gung University, Taiwan, in 2014 and Colorado State University in 2017, respectively. He is currently a Ph.D. student at Colorado State University. His research interests focus on the development of integrated sensor systems for monitoring metabolism of cells. This includes biosensor chip design and sensor circuit design.

**Adam Chicco** is an associate professor in the Department of Biomedical Sciences at Colorado State University and Fellow of the American Heart Association. He received his PhD at the University of Northern Colorado and developed an interest in the links between metabolism and cardiovascular physiology during his postdoctoral training at the University of Colorado. The current focus of his laboratory is to understand the mechanisms and (patho)physiological consequences of altered mitochondrial function and fatty acid metabolism in the context of physiological and pathological stress. His has expertise in high resolution respirometry enabling detailed studies of mitochondrial metabolism in a variety of sample preparations, and is a member of the Mitochondrial Physiology Network, an international group of scientists that strive to maintain and establish new standards of mitochondrial respirometry methodology, data reproducibility, and interpretation. His research has been continuously funded by the US National Institutes of Health, American Heart Association, US Department of Agriculture, and private foundations since 2005; and includes collaborative studies of mitochondrial metabolism in the contexts of environmental stress, developmental metabolic programming, and inflammation.

**Daniel Ball** received the B.S. degree in computer engineering from Colorado State University, Fort Collins, CO, USA, in 2017, and the M.S. degree in electrical engineering from Colorado State University in 2021. From 2014 to 2017 he was an Undergraduate Research Assistant with the Melange research group at Colorado State University. From 2017 to 2021 he was a Graduate Research Assistant for the BLISS research group at Colorado State University. He is currently a Research Associate for the BLISS research group at Colorado State University.

**Tom Chen** is a professor at the Department of Electrical and Computer Engineering (ECE) and School of Biomedical Engineering (SBME). He received his B.S. from Shanghai Jiaotong University and Ph.D. from the University of Edinburgh. He spent 4 years with Philips Semiconductors in Europe and 1 year with New Jersey Institute of Technology before joining Colorado State University. His research interests include all aspects of biosensors and bioelectronics and their applications to biology and biomedical sciences. Dr. Chen has over 150 refereed journal and conference publications in the areas of VLSI circuits and biosensor circuits and systems, and 4 US patents. Dr. Chen provided expert opinions for the Federal Trade Commission, and guest edited several IEEE and Elsvier journal issues on CMOS circuit designs and microelectronics. Dr. Chen is a senior member of IEEE and a member of the Steering Committee for IEEE Midwest Symposium on Circuits and Systems. He currently holds Business Challenge Endowment Professorship at Colorado State University.